Recombinant *Escherichia coli* as a biofactory for various single- and multi-element nanomaterials

Yoojin Choi[a,b,c,d], Tae Jung Park[e,1], Doh C. Lee[d], and Sang Yup Lee[a,b,c,d,1]

[a]Metabolic and Biomolecular Engineering National Research Laboratory, Korea Advanced Institute of Science and Technology, Yuseong-gu, 34141 Daejeon, Republic of Korea; [b]BioProcess Engineering Research Center, Korea Advanced Institute of Science and Technology, Yuseong-gu, 34141 Daejeon, Republic of Korea; [c]Institute for the BioCentury, Korea Advanced Institute of Science and Technology, Yuseong-gu, 34141 Daejeon, Republic of Korea; [d]Department of Chemical and Biomolecular Engineering (BK21 Plus Program), Korea Advanced Institute of Science and Technology, Yuseong-gu, 34141 Daejeon, Republic of Korea; and [e]Department of Chemistry, Research Institute for Halal Industrialization Technology, Chung-Ang University, Dongjak-gu, 06974 Seoul, Republic of Korea

Contributed by Sang Yup Lee, April 27, 2018 (sent for review March 16, 2018; reviewed by Francois Baneyx and Antonio Villaverde)

Nanomaterials (NMs) are mostly synthesized by chemical and physical methods, but biological synthesis is also receiving great attention. However, the mechanisms for biological producibility of NMs, crystalline versus amorphous, are not yet understood. Here we report biosynthesis of 60 different NMs by employing a recombinant *Escherichia coli* strain coexpressing metallothionein, a metal-binding protein, and phytochelatin synthase that synthesizes a metal-binding peptide phytochelatin. Both an in vivo method employing live cells and an in vitro method employing the cell extract are used to synthesize NMs. The periodic table is scanned to select 35 suitable elements, followed by biosynthesis of their NMs. Nine crystalline single-elements of Mn_3O_4, Fe_3O_4, Cu_2O, Mo, Ag, $In(OH)_3$, SnO_2, Te, and Au are synthesized, while the other 16 elements result in biosynthesis of amorphous NMs or no NM synthesis. Producibility and crystallinity of the NMs are analyzed using a Pourbaix diagram that predicts the stable chemical species of each element for NM biosynthesis by varying reduction potential and pH. Based on the analyses, the initial pH of reactions is changed from 6.5 to 7.5, resulting in biosynthesis of various crystalline NMs of those previously amorphous or not-synthesized ones. This strategy is extended to biosynthesize multi-element NMs including $CoFe_2O_4$, $NiFe_2O_4$, $ZnMn_2O_4$, $ZnFe_2O_4$, Ag_2S, Ag_2TeO_3, Ag_2WO_4, Hg_3TeO_6, $PbMoO_4$, $PbWO_4$, and $Pb_5(VO_4)_3OH$ NMs. The strategy described here allows biosynthesis of NMs with various properties, providing a platform for manufacturing various NMs in an environmentally friendly manner.

biosynthesis | nanomaterials | *Escherichia coli* | single element | multi-element

Nanomaterials (NMs) (1) such as metal nanoparticles, metal nanorods, carbon nanotubes, and graphene are indispensably used in many industries (2) including electronics, energy, chemicals, and medicine because of their unique electric, optical, and catalytic properties depending on their composition, size, and shape (3, 4). There has been much interest in producing diverse NMs that can be used for old and new applications in various fields (5–7). NMs are mostly synthesized by rather energy intensive chemical and physical methods (e.g., hydrothermal, sonochemical, and microwave irradiation) at high temperature (60–950 °C) and pressure (~1,000 bar), which also typically requires hazardous toxic capping agents (e.g., polyetherimide and polyacrylic acid) and solvents (e.g., toluene and oleyl amine) to disperse and purify NMs after synthesis (8, 9). Thus, biosynthesis and purification of NMs under mild conditions using nontoxic solvents (mostly water) without requiring physical and chemical treatments has attracted much attention (10).

There have been numerous studies on the biosynthesis of NMs, mostly including noble metal (Pd, Ag, Au, and Pt) and transition metal (Mn, Fe, Cu, Zn, Se, and Cd) elements, that employ plant extracts, bacteria, fungi, and yeast (10–13). The use of bacteria, which grow much faster than fungi and yeast, as NM biofactories has attracted much attention (14). Also, the use of bacteria is better than using plant extract (*SI Appendix*, *Text S1*). Bioreduction of the exposed precursor ions by bacteria results in precipitation of insoluble complexes, forming NMs in some cases. For example, the wild-type *Escherichia coli* cells have been successfully employed to synthesize NMs of noble metal (Ag and Au) and transition metal (Cu, Se, and Cd) elements (10). Although the exact mechanisms of associated microbial proteins for NM biosynthesis are not clear, metallothionein (MT), one of the well-known metal-binding proteins, and phytochelatin (PC) synthesized by phytochelatin synthase (PCS) have been relatively well characterized. The MT and PC have been investigated for their roles in the biosynthesis of NMs. MT is a low-molecular-weight, metal-binding protein, which can bind heavy metals (i.e., Cu, Zn, and Cd) through clusters of thiolate bonds (15). PC is a family of cysteine-rich, thiol-reactive peptides that bind several toxic metals (i.e., Cu, Zn, Cu, Hg, and Pb). It plays an important role in heavy-metal detoxification processes (16). As PCS can be generally overexpressed in cells when exposed to metal ions, PCs are synthesized and form complexes with the metal ions via metal binding and reduction (17). Both MT and PC are rich in

Significance

Nanomaterials (NMs) including metals, metal oxides, and quantum dots are increasingly used for developing various materials of industrial use. Conventional NM synthesis by chemical and physical methods requires rather harsh and environmentally hazardous conditions. Here we report biosynthesis of various NMs by employing a recombinant *Escherichia coli* strain co-expressing metallothionein and phytochelatin synthase. A Pourbaix diagram was employed to predict producibility and crystallinity of NMs. We were able to synthesize 60 different crystalline and amorphous NMs comprising a single-element or multi-elements, including those never biosynthesized or synthesized chemically before. The biosynthesized NMs were analyzed for their size, shape, composition, and other characteristics. The strategy reported here will be useful for producing under mild conditions various single- and multi-element NMs for industrial use.

Author contributions: S.Y.L. conceived the project; S.Y.L. designed research; Y.C. and T.J.P. performed research; Y.C., T.J.P., D.C.L., and S.Y.L. analyzed data; and Y.C., T.J.P., D.C.L., and S.Y.L. wrote the paper.

Reviewers: F.B., University of Washington; and A.V., Autonomous University of Barcelona.

Conflict of interest statement: S.Y.L., T.J.P., and Y.C. are the inventors of patents filed on the biosynthesis of various nanomaterials (KR10-0755746, US8476055, IN249926, KR10-2016-0182245, and PCT/KR2016/015498) for potential commercialization.

[1]To whom correspondence may be addressed. Email: leesy@kaist.ac.kr or tjpark@cau.ac.kr.

This article contains supporting information online at www.pnas.org/lookup/suppl/doi:10.1073/pnas.1804543115/-/DCSupplemental.

Published online May 21, 2018.

cysteins, the thiol group of which act as a reducing agent for the formation of NMs (10, 16). For these reasons, MT and/or PC have been employed to biosynthesize various metal NMs (13, 18–20). For example, the biosynthesis of cadmium sulfide NM by recombinant *E. coli* expressing the *Schizosaccharomyces pombe* PCS gene and the γ-glutamylcysteine synthetase gene has been reported (13). Also, we previously developed a recombinant *E. coli* strain coexpressing MT and PCS, which allowed biosynthesis of more diverse NMs with higher efficiencies compared with the method employing either MT or PCS alone (*SI Appendix*, *Text S2*) (18–20).

Despite the promising potential of NM biosynthesis for producing various NMs, the exact capacity of the biosynthetic systems for producing a range of diverse NMs has not yet been fully explored. Thus, we became interested in exploring the biological synthetic capacity of NMs including NMs that have never been biosynthesized. Here we report biosynthesis of 60 different NMs covering 35 elements using a recombinant *E. coli* strain coexpressing MT and PCS as a NM biofactory. Biosynthesis of particular types of NMs, including producibility and crystallinity, can be explained and predicted by a Pourbaix diagram, which was subsequently used for the biosynthesis of stable NMs for each element by varying the reduction potential (Eh) and pH.

Results and Discussion

We first scanned through the periodic table to select 34 elements (excluding sulfur) for the biosynthesis of corresponding NMs (Fig. 1*A*). Elements such as diatomic nonmetals, noble gasses, precious and costly elements, major components and major essential cations of the cell, elements of which precursors soluble in water are unavailable, and radioactive elements were excluded from the precursor candidates in this work. Both the in vivo NM biosynthetic method employing the recombinant *E. coli* DH5α cells harboring pYJ-MT-PCS and the in vitro NM biosynthetic method using the cell extract of the same recombinant *E. coli* were employed for the biosynthesis of various single- and multi-element NMs (Fig. 1*B* and *SI Appendix*, Table S1). The use of the in vitro method is preferred (19) for the biosynthesis of NMs composed of highly toxic metal elements compared with the in vivo method (*SI Appendix*, Fig. S1). The producibility of the NMs and the crystallinity and physicochemical characteristics of NMs biosynthesized by both methods were studied.

Among the 34 elements examined, the recombinant *E. coli* DH5α cells harboring pYJ-MT-PCS synthesized either crystalline or amorphous NMs for 21 elements. Eight crystalline NMs synthesized in vivo were Mn_3O_4, Fe_3O_4, Cu_2O, Ag, $In(OH)_3$, SnO_2, Te, and Au (Fig. 1*C* and *SI Appendix*, Figs. S2–S4). In addition, a crystalline NM including Mo was produced through in vivo synthesis. However, its exact crystal structure could not be determined; lattice spacing (0.23 nm) was observed using transmission electron microscopy (TEM; *SI Appendix*, Fig. S2), but X-ray diffractometer (XRD) patterns were not clear enough to

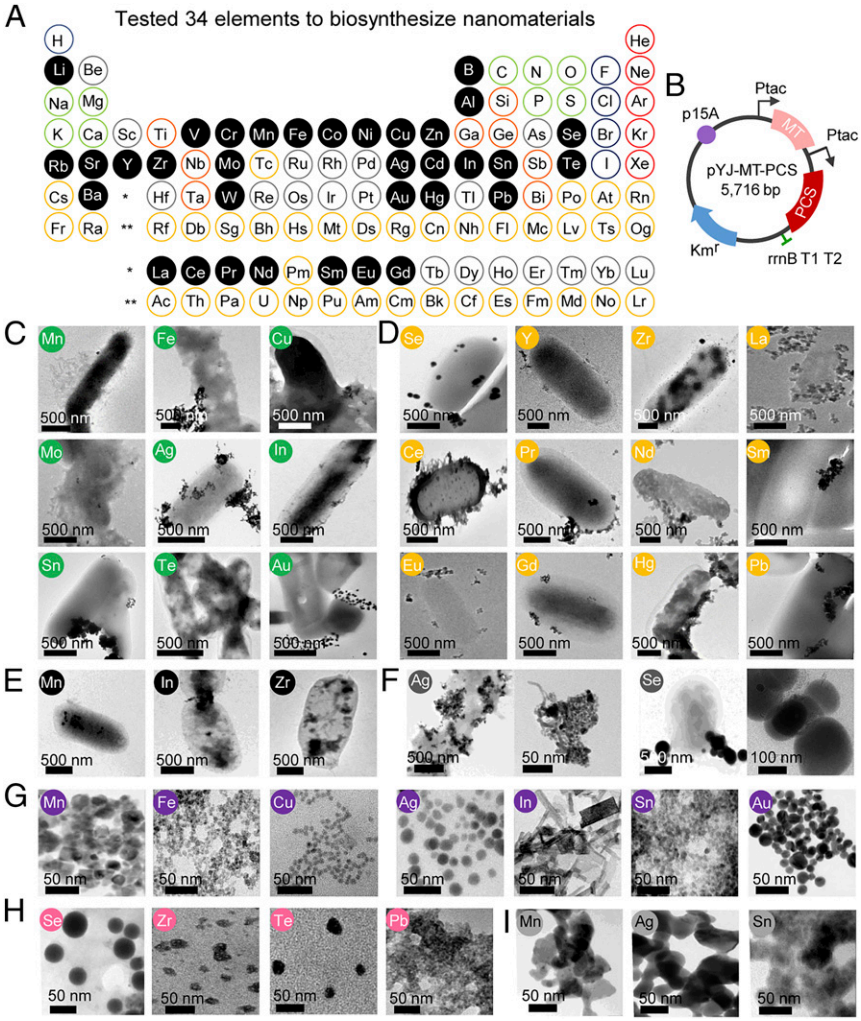

Fig. 1. In vivo and in vitro biosynthesis of various single-element NMs. (*A*) Thirty-four single elements (shown in the black closed circle) tested to biosynthesize various NMs are shown in the latest version of the Periodic Table (November 28, 2016) from the International Union of Pure and Applied Chemistry (https://iupac.org/what-we-do/periodic-table-of-elements/). Elements such as diatomic nonmetals (blue border circle), noble gasses (red border circle), precious and expensive elements (gray border circle), major components of biomolecules and essential cations of the cell (light-green border circle) (37) and elements having insoluble precursors (orange border circle) and radioactive elements (yellow border circle) were excluded from the precursor candidates in this work. (*B*) The map of plasmid pYJ-MT-PCS used to construct recombinant *E. coli* DH5α strain employed in 34 single-element screenings for the biosynthesis of NMs. In vivo reactions were performed for 12 h unless indicated specifically. MT and PCS are coexpressed from each plasmid under the separate *tac* promoter. (*C*) TEM images of nine crystalline NMs synthesized in vivo with their corresponding elements labeled in green circle. (*D*) TEM images of 12 amorphous NMs synthesized in vivo with their corresponding elements labeled in yellow circle. (*E*) TEM images of crystalline Mn_3O_4 and In $(OH)_3$ NMs and amorphous Zr NM synthesized in vivo by a 6-h reaction with their corresponding elements labeled in black circle. (*F*) TEM images of crystalline Ag NM and amorphous Se NM synthesized in vivo using a control *E. coli* DH5α strain harboring an empty vector pTac15K with their corresponding elements labeled in dark-gray circle. (*G*) TEM images of seven crystalline NMs synthesized in vitro with their corresponding elements labeled in purple circle. (*H*) TEM images of four amorphous NMs synthesized in vitro with their corresponding elements labeled in pink circle. (*I*) TEM images of crystalline Mn_3O_4, Ag, and SnO_2 NMs synthesized in vitro using the cell extract of the control *E. coli* strain harboring an empty vector with their corresponding elements labeled in light-gray circle.

confirm the crystal structure. However, the following 12 elements formed amorphous NMs through in vivo synthesis: Se, Zr, Hg, Pb, and lanthanides (La, Ce, Pr, Nd, Sm, Eu and Gd) (Fig. 1*D* and *SI Appendix*, Fig. S5). The other 13 elements, including Li, B, Al, V, Cr, Co, Ni, Zn, Rb, Sr, Cd, Ba and W, resulted in no NM synthesis in vivo. Most of crystalline and amorphous NMs synthesized in vivo after 12 h cultivation were observed on the surface of the cell membrane under TEM (Fig. 1 *C* and *D*), raising a question about the involvement of MT and PC in the biosynthesis of NMs. We provided detailed explanations on the locations of NMs biosynthesized in vivo (Fig. 1 *E* and *F*) and the roles of MT and PCS to biosynthesize monodispersed NMs. During the synthesis of crystalline Mn_3O_4 and $In(OH)_3$ NMs and amorphous Zr NM, for example, the NMs were mostly synthesized and located inside the cells at 6 h of cultivation (Fig. 1*E*), whereas most were found outside the cell membrane at 12 h of cultivation. Although the reason is not clear, such transport of NM has been previously reported (21). These results suggest that biosynthesis of NMs begins inside the cell, where MT and PC are present, and then NMs move to the cell wall, where biosynthesis continues. Moreover, during the nucleation process of NM, PCs serve as a binding template and nucleation site for the metal ions and stabilize the NM to prevent continued aggregation (13). To see if cells not expressing MT and PCS are also able to biosynthesize NMs, the control *E. coli* DH5α strain harboring an empty vector pTac15K was cultured and incubated with Ag and Se. Crystalline Ag NM and amorphous Se NM were biosynthesized, but the resulting NMs were heterogeneous in size and shape and tended to aggregate to each other (Fig. 1*F*). Because the NMs synthesized using the recombinant *E. coli* strain coexpressing MT and PCS were homogenous and well dispersed, MT and PC indeed can be said to facilitate NM biosynthesis and stabilization (*SI Appendix*, *Text S3* and Fig. S6).

Through in vitro synthesis, 11 of 34 elements successfully formed either crystalline or amorphous NMs (Fig. 1 *G* and *H* and *SI Appendix*, Figs. S7–S9); detailed results are shown in *SI Appendix*, *Text S4*. These results clearly show that NMs are more readily biosynthesized in vivo than in vitro (formation of 21 and 11 NMs, respectively). Since nicotinamide adenine dinucleotide (NADH) has been reported to provide reducing power during the biosynthesis of NMs (21–23), we chose NADH concentration as an indicator for the level of available reducing power during the synthesis of NMs. The NADH level in vivo increased during the cultivation of recombinant *E. coli*, while that of the cell extract stayed relatively constant during the incubation (*SI Appendix*, Fig. S10). In addition, the NADH level in the recombinant cells was 3.5 times higher than that of the cell extract after 12 h of incubation. Thus, MT and PC can biosynthesize NMs more efficiently in vivo where more NADH is available.

To understand why some elements led to biosynthesis of NMs while others did not in vivo and/or in vitro (e.g., NM producibility), Pourbaix diagram analysis was performed for predicting the stability and predominant forms of elements through the calculation of the effects of Eh and pH values (Fig. 2*A* and *SI Appendix*, *Text S5*) (24, 25). The results of the Pourbaix diagram analyses were consistent with the in vivo experimental results; the NM biosynthesis of the correct product for 21 elements was confirmed (*SI Appendix*, Figs. S9 and S10). No NM biosynthesis for nine elements was also consistent with the results of Pourbaix diagram analysis (*SI Appendix*, Fig. S13). However, no NM biosynthesis for four elements (B, Al, V, and Cr) in our experiments could not be explained by the Pourbaix diagram, which suggested the possible formation of $B(OH)_3$, V_6O_{13}, V_2O_4, V_3O_5, V_2O_3, $Al(OH)_3$, and Cr_2O_3, respectively. Similarly, Pourbaix diagram analyses were also performed for in vitro synthesis of NMs (*SI Appendix*, *Text S6* and Figs. S15–S17).

Detailed examination of the Pourbaix diagrams of Cd, Ni, Zn, and Cd suggested that they could form crystalline NMs at pH 7.5 (*SI Appendix*, Fig. S17). Thus, the initial pH of the in vivo NM biosynthesis reactions was shifted to 7.5. In addition, the same strategy was applied to 12 elements that formed amorphous NMs to see whether crystalline NMs could be formed at pH 7.5 (*SI Appendix*, Fig. S12). The other four reactions with no NM synthesis were excluded since the ionic states of the elements (Li^+, Rb^+, Sr^{2+}, and WO_4^{2-}) were dominant forms over the examined pH range of 6–10 (*SI Appendix*, Fig. S13). At pH 7.5, 10 crystalline NMs, β$Ni(OH)_2$, ZnO, β-$Cd(OH)_2$, $BaCO_3$, $La(OH)_3$, $Pr(OH)_3$, $Nd(OH)_3$, $Sm(OH)_3$, $Eu(OH)_3$, and $Gd(OH)_3$ were successfully synthesized (Fig. 2*B* and *SI Appendix*, Figs. S19 and S20). In the case of Co and Ce, two separate single-element crystalline NMs were synthesized in vivo at pH 7.5 for each: β-$Co(OH)_2$ and Co_3O_4; $Ce(OH)_3$ and CeO_2 (*SI Appendix*, *Text S7* and Fig. S19*B*). In the case of Se, Y, Zr, Hg, and Pb, five amorphous NMs were formed in vivo at pH 7.5 (Fig. 2*C* and *SI Appendix*, Figs. S20*A* and S21). However, no NMs were synthesized for B, Al, V, and Cr even at pH 7.5 (*SI Appendix*, Fig. S20*B*). Next, the same strategy of increasing the initial pH to 7.5 was applied to in vitro NM synthesis. Various single-element crystalline and amorphous NMs were obtained at pH 7.5 (Fig. 2 *D* and *E* and *SI Appendix*, *Text S8* and Figs. S22–S28).

Using the in vivo and in vitro methods described above, we were able to biosynthesize the crystalline MoO_2, $In(OH)_3$, $La(OH)_3$, $Ce(OH)_3$, $Pr(OH)_3$, $Nd(OH)_3$, $Sm(OH)_3$, $Eu(OH)_3$, $Gd(OH)_3$, $Pb_3(NO)_3(OH)_5$, and $Pb_3(NO)_3(OH)_5$ NMs and amorphous Y, Ce, Pr, Nd, Sm, Eu, Gd, Hg, and Pb NMs. Although the Pourbaix diagram predicted crystalline NMs for Se, $Y(OH)_3$, ZrO_2, and $Pb(OH)_2$ by the in vivo method (Fig. 2*C* and *SI Appendix*, Fig. S21) and Se, $Y(OH)_3$, ZrO_2, and Te by the in vitro method (Fig. 2*E* and *SI Appendix*, Fig. S28), amorphous NMs were biosynthesized despite changing the initial pH to 7.5 (*SI Appendix*, *Text S9*). These elements will require further studies to better understand the mechanisms that underlie the formation of NMs with respect to crystallinity and producibility. Formation of crystalline materials and transformation of amorphous to crystalline materials have been investigated for metal, metal oxide, and semiconducting NMs and also geologic and biologic minerals (26–29); in some cases, kinetic and energetic factors were considered and explained. In this study, we employed the Pourbaix diagram analyses for predicting producibility and crystallinity of NMs from the thermodynamic aspect. Although we did not systematically investigate kinetic and energetic factors during NM biosynthesis mainly because the reactions were performed at mild temperature, more studies on time- and temperature-dependent biosynthesis would result in better understanding of NM biosynthesis in kinetic and energetic points of view in the future.

In the case of Fe, the Pourbaix diagram suggests that two different types of crystalline Fe NMs, Fe_3O_4 and Fe_2O_3 (the former was the Fe NM synthesized by in vitro reactions at pH 6.5; Fig. 1 *C* and *G* and *SI Appendix*, Figs. S3*B* and S8*B*), can be synthesized at different reduction potentials. To obtain pure α-Fe_2O_3 NM, the two by-products of β-FeOOH and α-FeOOH and the recombinant cells were removed by calcination at a high temperature of 800 °C. Examination of the changes of Eh and pH during the in vivo and in vitro reactions suggested that a 6-h reaction would give the Eh value suitable for the biosynthesis of α-Fe_2O_3 NM (*SI Appendix*, Fig. S29); this was experimentally verified (*SI Appendix*, *Text S10* and Figs. S30 and S31).

To further extend the spectrum of NMs, biosynthesis of two-element NMs and three-element NMs including oxygen was attempted by in vivo and in vitro reactions. We tested combinations of 35 elements including S as it is a component of various metal sulfide-based NMs. To forward-predict producible chemical species in each reaction, we analyzed Pourbaix diagrams of

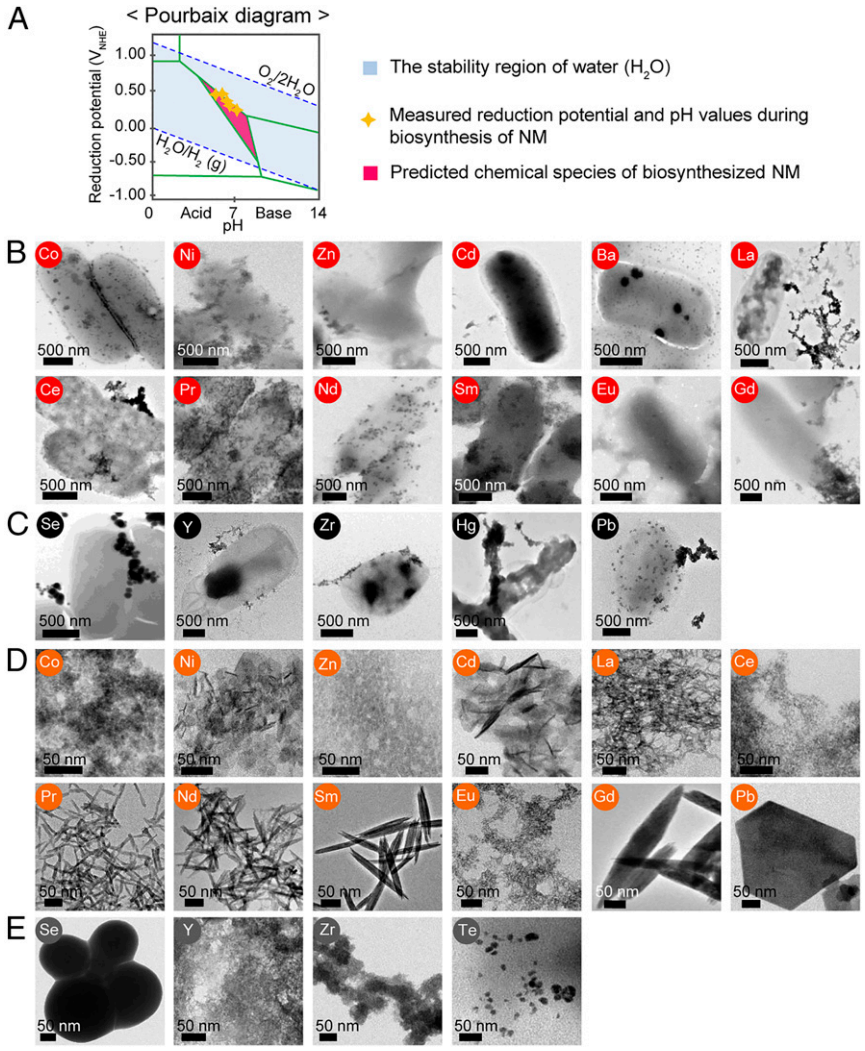

Fig. 2. A schematic of Pourbaix diagram and various NMs biosynthesized in vivo and in vitro at the initial pH of 7.5. (*A*) A schematic of Pourbaix diagram indicates stable chemical species (e.g., types of element) at a given Eh and pH in an aqueous solution. The upper blue dashed line denotes the reduction potential of the oxygen evolution reaction, while the lower blue dashed line corresponds to the reduction potential of the hydrogen evolution reaction. The light-blue area represents the Eh and pH range available in stable water (38). Green boundaries illustrate the points where two different chemical species coexist forming an equilibrium. Yellow stars represent Eh and pH values experimentally measured during the 12-h period of NM biosynthesis. The pink region is where the predicted chemical species exist for the biosynthesis of NMs comprising them. Based on the Pourbaix diagram analysis, the producibility and crystallinity of NMs were examined in aqueous solution. (*B*) TEM images of 12 crystalline NMs synthesized in vivo at pH 7.5 with their corresponding elements labeled in red circle. (*C*) TEM images of five amorphous NMs synthesized in vivo at pH 7.5 with their corresponding elements labeled in black circle. (*D*) TEM images of 12 crystalline NMs synthesized in vitro at pH 7.5 with their corresponding elements labeled in orange circle. (*E*) TEM images of four amorphous NMs synthesized in vitro at pH 7.5 with their corresponding elements labeled in dark-gray circle.

595 possible bielemental combinations (*SI Appendix*, Figs. S32–S34 and Dataset S1). While 47 of the 595 combinations were predicted to produce compounds involving both precursor elements in the Eh and pH ranges of −1.0461 ∼ +1.0461 V and 6 ∼ 10, respectively, only 34 combinations were predicted to be synthesizable as crystalline NMs under in vivo biosynthesis conditions (*SI Appendix*, Figs. S32 and S33). Among these 34 combinations, crystalline CdSe and ZnSe NMs have previously been biosynthesized (18). Among the other 32 bielemental combinations, 16 of them, including Al/S, S/Co, S/Mo, S/Ag, V/Ag, V/Pb, Cr/Zn, Fe/Co, Fe/Ni, Fe/Zn, Cu/Se, Se/Sr, Se/Ag, Mo/Pb, Ag/W, and W/Pb, were selected for proof-of-concept in vivo biosynthesis (*SI Appendix*, Fig. S32). Seven multi-element crystalline NM [i.e., Ag_2S, $CoFe_2O_4$, $NiFe_2O_4$ (together with β-FeOOH as a by-product), $ZnFe_2O_4$, $PbMoO_4$, γ-Ag_2WO_4 (together with β-Ag_2WO_4), and $PbWO_4$ (together with W_5O_{14})] were biosynthesized as predicted from Pourbaix diagram analyses (Fig. 3*A* and *SI Appendix*, Figs. S35 and S36*A*). For the other combinations, single crystalline or amorphous NMs were formed in some cases, or no NM was formed for the others (*SI Appendix*, *Text S11* and Figs. S32 and S37).

Next, among the 548 combinations that were predicted to form no multi-element NMs according to the Pourbaix diagram (Dataset S1), we examined the producibility of 42 bielemental combinations (*SI Appendix*, *Text S12* and Fig. S34). Interestingly, crystalline $ZnMn_2O_4$ (together with $ZnMnO_3$), Ag_2TeO_3, and Hg_3TeO_6 NMs were in vivo-synthesized (Fig. 3*B* and *SI Appendix*, Figs. S34*A*, S36*B*, and S38), suggesting that not many, but some, multi-element NMs that were predicted not producible from Pourbaix diagram analysis could also be biosynthesized. For the other combinations, either single crystalline or amorphous NMs or no NM formation was observed (*SI Appendix*, *Text S13* and Figs. S34 and S37).

Next, the in vitro biosynthesis of the same bielemental combinations was performed. Ten multi-element crystalline NMs were in vitro-biosynthesized, including Ag_2S, $CoFe_2O_4$, $NiFe_2O_4$ (together with β-FeOOH as a by-product), $ZnFe_2O_4$, $PbMoO_4$, β-Ag_2WO_4, $PbWO_4$, $ZnMn_2O_4$, Ag_2TeO_3, and Hg_3TeO_6 (Fig. 3*C* and *SI Appendix*, Figs. S36*C* and S39); these are multi-element NMs previously formed by in vivo reactions as well. For the other combinations, either single crystalline or amorphous NMs or no NM formation was observed (*SI Appendix*, *Text S14* and Fig. S40). As done for single-element NMs, biosynthesis of multi-element NMs at pH 7.5 was also performed (Fig. 3 *D* and *E* and *SI Appendix*, Text S15 and Figs. S36 and S41–S45). In summary, the pH shift experiment resulted in biosynthesis of seven more multi-element NMs including crystalline Na_4VO_2, Na_4CrO_4, Na_3AgO_2, CoO(OH), $Zn(OH)_2$, Ag_2O, and $Pb_5(VO_4)_3OH$ NMs.

Taken together, the in vivo and in vitro NM biosynthesis methods reported here resulted in the synthesis of 18 crystalline multi-element NMs (Fig. 3). The crystal structures of 10 multi-element crystalline NMs could be reconstructed based on the XRD data (*SI Appendix*, Fig. S45). Among the 18 NMs, 13 of them including Na_4VO_2, Na_4CrO_4, Na_3AgO_2, $NiFe_2O_4$, $Zn(OH)_2$, $ZnMn_2O_4$, Ag_2TeO_3, Ag_2WO_4, W_5O_{14}, Hg_3TeO_6, $PbMoO_4$, $PbWO_4$, and $Pb_5(VO_4)_3OH$ were biosynthesized in this study. Notably, crystalline Ag_2TeO_3 NM biosynthesized both in vivo and in vitro was never synthesized before by chemical or biological means. Since this is a novel NM, more detailed studies were performed. As the size of single-element NM could be modulated by changing the concentration of the precursor element (18), we wanted to know whether the size of multi-element NM could also be modulated. It was found that the size of NM could be varied from 13.69 ± 0.87 nm to 34.96 ± 1.38 nm by increasing the precursor concentrations from 0.25 to 2.0 mM (*SI Appendix*, Figs. S46 and S47), suggesting that the size of multi-element NM could also be modulated as desired. The overall results of in vivo and in vitro biosynthesis of various single- and multi-element NMs are summarized in *SI Appendix*, Fig. S48 and Dataset S2. Also, their characteristics (i.e., chemical composition, size, and shape) are presented in *SI Appendix*, Table S2. As can be seen from these results, NMs biosynthesized exhibited various sizes and shapes. Although the exact mechanisms for such variations are not fully understood, different rates of metal ion uptake, reduction, and crystal growth are most likely the reasons.

One of the characteristics of NM biosynthesis is that there are functional groups originating from biomolecules on the surface of NMs. To identify the surface functional groups of biosynthesized NMs, Fourier transform infrared (FTIR) spectroscopy analysis was performed. The FTIR data showed that biomolecules were present and attached on the surface of the biosynthesized NMs (*SI Appendix*, Figs. S49–S53). For both in vivo- and in vitro-biosynthesized NMs, appearance of peaks in FTIR corresponding to amino acid bond vibrations typically observed for proteins and peptides (30) suggested that some amide groups existed on the surface of biosynthesized NMs. The C-H bond peak appearing at ∼2,900 cm^{-1} was from aliphatic compounds in the cell membrane (*SI Appendix*, Figs. S49–S51), which was stronger for in vivo-biosynthesized NMs compared with in vitro-biosynthesized NMs (*SI Appendix*, Figs. S52 and S53). Biosynthesized NMs were surrounded by various functional groups of biomolecules, including O-H (3,300–3,000 cm^{-1}), C-H (2,960–2,850 cm^{-1}), amide groups (1,660–1,650 cm^{-1}, 1,540–1,535 cm^{-1}, and 1,240–1,234 cm^{-1}, amide I, amide II, and amide III, respectively), and C = O (1,155–1,030 cm^{-1}) peaks (30). Such modification of NMs with functional groups originating from various cellular biomolecules, including MT and PCS, seems to be involved in the stabilization of NMs.

Among the various NMs biosynthesized in this study, magnetic NMs including Mn_3O_4, Fe_3O_4, $CoFe_2O_4$, $NiFe_2O_4$, $ZnMn_2O_4$, and $ZnFe_2O_4$ were further characterized for their magnetic

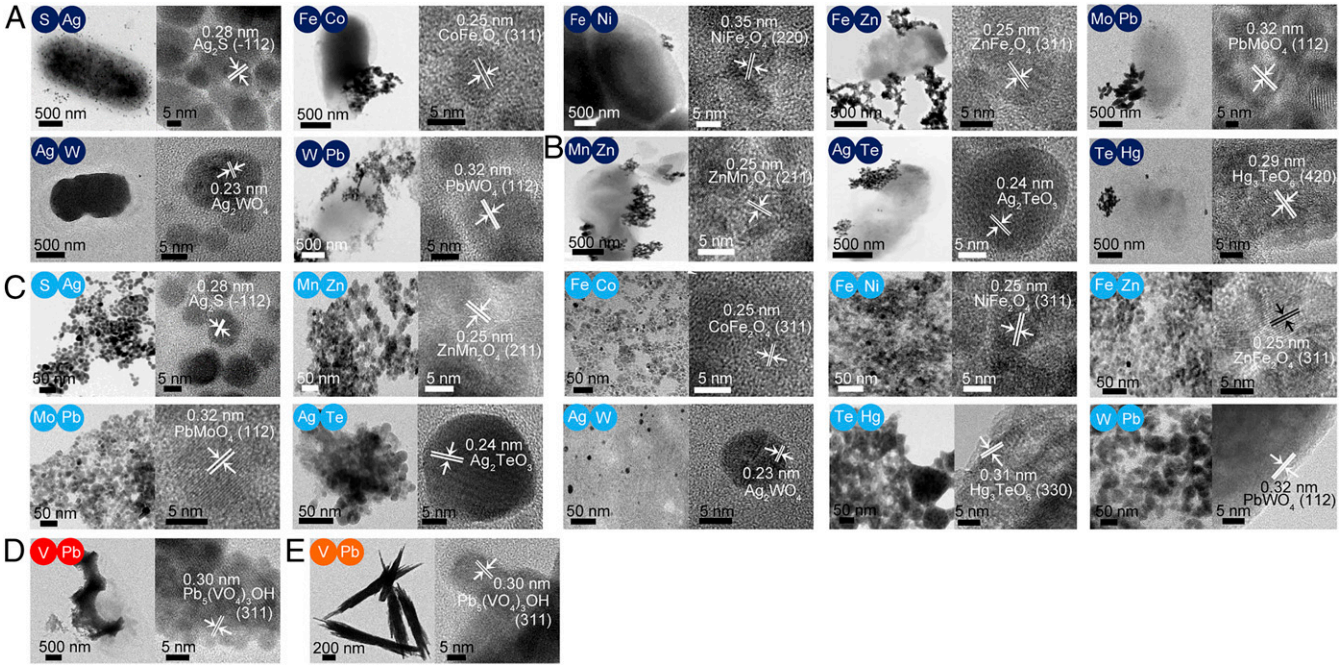

Fig. 3. In vivo and in vitro biosynthesis of multi-element crystalline NMs. For each result with indicated bielements: (*Left*) the TEM image and (*Right*) the HR-TEM image. In the HR-TEM image, the interplanar distance of the crystalline NM lattice and the Miller indices of crystallographic planes within parentheses are also shown. Corresponding elements are labeled in colored circles. (*A*) Seven multi-element NMs synthesized in vivo. (*B*) Three multi-element NMs synthesized in vivo. These NMs were predicted to be not producible from Pourbaix diagram analysis but could be biosynthesized. (*C*) Eight multi-element NMs synthesized in vitro. (*D*) $Pb_5(VO_4)_3OH$ NM synthesized in vivo at pH 7.5. (*E*) $Pb_5(VO_4)_3OH$ NM synthesized in vitro at pH 7.5.

properties at 300 K (*SI Appendix*, Fig. S54). Crystalline Mn_3O_4 and Fe_3O_4 NMs biosynthesized in this study showed paramagnetic and ferromagnetic properties, respectively. The multi-element NMs showed ferromagnetic ($CoFe_2O_4$ synthesized in vivo and in vitro and $NiFe_2O_4$ NMs synthesized in vivo), superparamagnetic ($NiFe_2O_4$ NM synthesized in vitro and $ZnFe_2O_4$ NM synthesized in vivo and in vitro), and paramagnetic ($ZnMn_2O_4$ NM synthesized in vivo and in vitro) properties. The in vitro-synthesized magnetic NMs were found to have higher saturation magnetization (*Ms*) values compared with the in vivo-synthesized NMs. This is due to the difference between the in vivo and in vitro biosynthesis methods (*SI Appendix*, *Text S16*). The *Ms* values increased for the in vivo-synthesized magnetic crystalline NMs due to the elimination of surface functional groups by calcination. The magnetic NMs having such diverse magnetic properties can be used in various biomedical fields (31), such as magnetic resonance imaging, biosensing, and anticancer drug delivery, because biosynthesized NM shows lower toxicity to living organisms compared with chemically synthesized NMs (32).

In summary, we demonstrated the biosynthesis of various NMs through the extensive screening of single elements and bielemental combinations during in vivo and in vitro biosynthesis using recombinant *E. coli* and the cell extract, respectively. We were able to synthesize 60 different NMs covering 35 elements, and among them, 33 previously unsynthesized NMs (20 single-element NMs and 13 multi-element NMs) including Ag_2TeO_3 were produced. The mechanism of producibility and crystallinity of NM biosynthesis could be predicted by Pourbaix diagram analyses in many cases, allowing the forward design of NM biosynthesis of single elements and multi-elements of interest. Various single- and multi-element NMs biosynthesized in this study can potentially serve as NMs for exciting industrial applications such as catalysts, gas sensors, biosensors, bioimaging, drug delivery, and cancer therapy (10, 32–36). There has been increasing interest in synthesizing various NMs that have not yet been synthesized for various applications including enhanced solar cells, semiconducting materials, biomedical materials, and many others. The strategies of NM biosynthesis described here will be useful for further diversifying the portfolio of NMs that can be manufactured.

Materials and Methods

All of the materials and methods conducted in this study are detailed in *SI Appendix, Materials and Methods*: bacterial strains and plasmids, induction of MT and PCS expression, expression of MT and PCS, in vivo synthesis of NMs, growth of recombinant *E. coli* in the presence of different precursors, preparation of cell extract, in vitro synthesis of NMs, in vivo synthesis of crystalline NMs at initial pH 7.5, in vitro synthesis of crystalline NM at initial pH 7.5, in vivo and in vitro synthesis of crystalline α-Fe_2O_3 NM, characterization of the biosynthesized NMs, generation of Pourbaix diagrams, measurement of Eh and pH, and measurement of NADH level.

The data supporting the findings of this study are available in the *SI Appendix*.

ACKNOWLEDGMENTS. We thank Professor H. U. Kim and K. R. Choi (Korea Advanced Institute of Science and Technology) for helpful discussion and Professor K. M. Ok (Chung-Ang University) for technical support into Joint Committee on Powder Diffraction Standards. This work was supported by the Technology Development Program to Solve Climate Changes on Systems Metabolic Engineering for Biorefineries from the Ministry of Science and ICT through the National Research Foundation of Korea (Grants NRF-2012M1A2A2026556 and NRF-2012M1A2A2026557).

1. Guozhong Cao YW (2011) *Nanostructures and Nanomaterials: Synthesis, Properties, and Applications* (World Scientific, Singapore).
2. Stark WJ, Stoessel PR, Wohlleben W, Hafner A (2015) Industrial applications of nanoparticles. *Chem Soc Rev* 44:5793–5805.
3. Lohse SE, Murphy CJ (2012) Applications of colloidal inorganic nanoparticles: From medicine to energy. *J Am Chem Soc* 134:15607–15620.
4. Yu X, Marks TJ, Facchetti A (2016) Metal oxides for optoelectronic applications. *Nat Mater* 15:383–396.
5. Chen P-C, et al. (2016) Polyelemental nanoparticle libraries. *Science* 352:1565–1569.
6. Davies DW, et al. (2016) Computational screening of all stoichiometric inorganic materials. *Chem* 1:617–627.
7. Edmundson MC, Capeness M, Horsfall L (2014) Exploring the potential of metallic nanoparticles within synthetic biology. *N Biotechnol* 31:572–578.
8. Duan H, Wang D, Li Y (2015) Green chemistry for nanoparticle synthesis. *Chem Soc Rev* 44:5778–5792.
9. Bekermann D, Barreca D, Gasparotto A, Maccato C (2012) Multi-component oxide nanosystems by chemical vapor deposition and related routes: Challenges and perspectives. *CrystEngComm* 14:6347–6358.
10. Park TJ, Lee KG, Lee SY (2016) Advances in microbial biosynthesis of metal nanoparticles. *Appl Microbiol Biotechnol* 100:521–534.
11. Huang J, et al. (2015) Bio-inspired synthesis of metal nanomaterials and applications. *Chem Soc Rev* 44:6330–6374.
12. Durán N, et al. (2011) Mechanistic aspects in the biogenic synthesis of extracellular metal nanoparticles by peptides, bacteria, fungi, and plants. *Appl Microbiol Biotechnol* 90:1609–1624.
13. Kang SH, Bozhilov KN, Myung NV, Mulchandani A, Chen W (2008) Microbial synthesis of CdS nanocrystals in genetically engineered *E. coli*. *Angew Chem Int Ed Engl* 47: 5186–5189.
14. Klaus-Joerger T, Joerger R, Olsson E, Granqvist C (2001) Bacteria as workers in the living factory: Metal-accumulating bacteria and their potential for materials science. *Trends Biotechnol* 19:15–20.
15. Hamer DH (1986) Metallothionein. *Annu Rev Biochem* 55:913–951.
16. Cobbett CS (2000) Phytochelatin biosynthesis and function in heavy-metal detoxification. *Curr Opin Plant Biol* 3:211–216.
17. Li Y, et al. (2004) Overexpression of phytochelatin synthase in Arabidopsis leads to enhanced arsenic tolerance and cadmium hypersensitivity. *Plant Cell Physiol* 45: 1787–1797.
18. Park TJ, Lee SY, Heo NS, Seo TS (2010) *In vivo* synthesis of diverse metal nanoparticles by recombinant Escherichia coli. *Angew Chem Int Ed Engl* 49:7019–7024.
19. Lee KG, et al. (2012) In vitro biosynthesis of metal nanoparticles in microdroplets. *ACS Nano* 6:6998–7008.
20. Kim EB, Seo JM, Kim GW, Lee SY, Park TJ (2016) *In vivo* synthesis of europium selenide nanoparticles and related cytotoxicity evaluation of human cells. *Enzyme Microb Technol* 95:201–208.
21. Singh R, Shedbalkar UU, Wadhwani SA, Chopade BA (2015) Bacteriagenic silver nanoparticles: Synthesis, mechanism, and applications. *Appl Microbiol Biotechnol* 99: 4579–4593.
22. Ahmad N, et al. (2011) Biosynthesis of silver nanoparticles from *Desmodium triflorum*: A novel approach towards weed utilization. *Biotechnol Res Int* 2011:454090.
23. Ahmad A, et al. (2002) Enzyme mediated extracellular synthesis of CdS nanoparticles by the fungus, Fusarium oxysporum. *J Am Chem Soc* 124:12108–12109.
24. Pourbaix M (1966) *Atlas of Electrochemical Equilibria in Aqueous Solutions* (Oxford Univ Press, Oxford).
25. Huang HH (2016) The Eh-pH diagram and its advances. *Metals (Basel)* 6:1–23.
26. De Yoreo JJ, et al. (2015) CRYSTAL GROWTH. Crystallization by particle attachment in synthetic, biogenic, and geologic environments. *Science* 349:aaa6760.
27. Koh, et al. (2017) Zinc–phosphorus complex working as an atomic valve for colloidal growth of monodisperse indium phosphide quantum dots. *Chem Mater* 29: 6346–6355..
28. Pak C, Lee DC (2012) Crystalline transformation of colloidal nanoparticles on graphene oxide. *ACS Appl Mater Interfaces* 4:1021–1029.
29. Gal A, et al. (2014) Particle accretion mechanism underlies biological crystal growth from an amorphous precursor phase. *Adv Funct Mater* 24:5420–5426.
30. Barth A (2007) Infrared spectroscopy of proteins. *Biochim Biophys Acta* 1767: 1073–1101.
31. Canfarotta F, Piletsky SA (2014) Engineered magnetic nanoparticles for biomedical applications. *Adv Healthc Mater* 3:160–175.
32. Seo JM, Kim EB, Hyun MS, Kim BB, Park TJ (2015) Self-assembly of biogenic gold nanoparticles and their use to enhance drug delivery into cells. *Colloids Surf B Biointerfaces* 135:27–34.
33. Kim I, et al. (2017) Virus-templated self-mineralization of ligand-free colloidal palladium nanostructures for high surface activity and stability. *Adv Funct Mater* 27: 1703262.
34. Choi Y, Hwang JH, Lee SY (2018) Recent trends in nanomaterials-based colorimetric detection of pathogenic bacteria and viruses. *Small Methods* 2:1700351.
35. Ali MRK, et al. (2017) Targeting cancer cell integrins using gold nanorods in photothermal therapy inhibits migration through affecting cytoskeletal proteins. *Proc Natl Acad Sci USA* 114:E5655–E5663.
36. Cherukula K, et al. (2016) Multifunctional inorganic nanoparticles: Recent progress in thermal therapy and imaging. *Nanomaterials (Basel)* 6:1–26.
37. Wackett LP, Dodge AG, Ellis LBM (2004) Microbial genomics and the periodic table. *Appl Environ Microbiol* 70:647–655.
38. Toma FM, et al. (2016) Mechanistic insights into chemical and photochemical transformations of bismuth vanadate photoanodes. *Nat Commun* 7:12012.